Journal of Statistical Physics, Vol. 65, Nos. 5/6, 1991

Trapping Aspects in Enhanced Diffusion

G. Zumofen,[1] J. Klafter,[2] and A. Blumen[3]

We study the superlinear diffusion $\langle x^2(t) \rangle \sim t^\alpha$, $\alpha > 1$, in layered media containing random velocity fields. The superlinear behavior holds in the case of random velocities along the x direction accompanied by diffusional motion in the space transverse to it. The transverse space can be either Euclidean, fractal, or ultrametric. For a one-dimensional transverse space we derive exact expressions for the higher moments of the displacement. Furthermore, we investigate the propagator $P(x, t)$ along the x direction and establish its scaling behavior. Our analysis highlights the resemblance between the stretched-Gaussian behavior of the propagator and the stretched-exponential form of the survivial probability in the trapping problem; both show late crossover behavior.

KEY WORDS: Diffusion; random velocity.

1. INTRODUCTION

There has been a growing interest in models of transport which exhibit enhanced diffusion; for this case the mean-squared displacement is superlinear:

$$\langle x^2(t) \rangle \sim t^\alpha, \qquad \alpha > 1 \tag{1}$$

Several models for enhanced diffusion have been proposed: (1) Generalizations of the diffusion equation by complex and sometimes nonlocal kernels.[1–6] (2) Deterministic maps.[7] (3) Lévy walks, an extension of the continuous-time random walk (CTRW) formalism.[8–13] (4) Models

This work is dedicated to Prof. George H. Weiss.

[1] Laboratorium für Physikalische Chemie, ETH-Zentrum, CH-8092 Zürich, Switzerland.
[2] School of Chemistry, Tel-Aviv University, Tel-Aviv, 69978 Israel.
[3] Physics Institute and BIMF, University of Bayreuth, D-8580 Bayreuth, Germany.

0022-4715/91/1200-0991$06.50/0

using the Matheron–de Marsily random velocity fields picture.[14–21] Experimental evidence for enhanced diffusion is found in turbulent fluids, for which typically $\alpha \simeq 3$.[1–4]

In this paper we focus on the Matheron–de Marsily model[14] (used to describe ground water flow in layered media) and on its extensions by Bouchaud *et al.*,[15] Mazo and Van den Broeck,[16] and Redner.[17] In fact, interest in motion in layered media is growing.[18–22] For the Matheron–de Marsily model α equals 3/2.

We consider a particle moving the longitudinal (x) and in the transverse (y) directions. The motion in the y direction is taken to be diffusional and to depend on the structure of the transverse space, which may be one-dimensional, fractal, ultrametric (UMS), etc., as demonstrated in Fig. 1. On the other hand, in the longitudinal x direction the direction of the motion is preassigned, being a function of y-dependent velocities. The velocities are randomly chosen, but kept fixed for a particular realization of the walk. Hence, the displacement of a random walker in the longitudinal direction is given through

$$x(t) = \int_0^t v[\mathbf{y}(t')]\, dt' \tag{2}$$

where $\mathbf{y}(t)$ denotes the y layer occupied by the walker at time t. Expression (2) was studied in detail in the occupancy problem by Darling and Kac[23] and by Kac.[24]

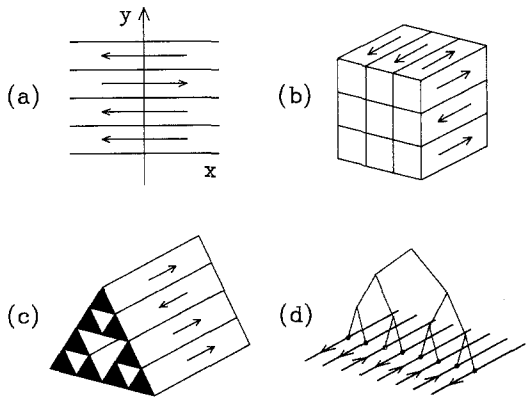

Fig. 1. Generalizations of the transverse motion. (a) The one-dimensional case, (b) the two-dimensional case, (c) the "Toblerone" structure with transverse motion on a Sierpinski gasket, (d) transverse motion on an ultrametric space. In all cases a possible realization for the longitudinal motion is indicated by arrows.

In this paper we choose dimensionless units (different from the convention introduced in ref. 21): lengths are given in units of a and velocities in units of a/τ, where a and τ are units of length and time, respectively. Furthermore, we choose the velocities of equal magnitude, but with random signs. This corresponds in configuration space to a δ-correlated field $v(\mathbf{y})$. Thus

$$\langle v(\mathbf{y})\, v(\mathbf{y}')\rangle_c = \delta_{\mathbf{y}\mathbf{y}'} \tag{3}$$

where $\delta_{\mathbf{y}\mathbf{y}'}$ denotes the Dirac delta function, i.e., for the continuum system $\delta_{\mathbf{y}\mathbf{y}'} = \delta(\mathbf{y}-\mathbf{y}')$. In Eq. (3) the average is taken over the velocity configurations.

This paper is structured as follows: in Section 2 we first consider a one-dimensional transverse space. For this we determine the moments of the $\langle x^m(t)\rangle$ and then treat the propagator $P(x, t)$. In Section 3 we generalize the model to systems for which the transverse motion takes place on fractals, on UMS, and higher-dimensional lattices. We end with conclusions in Section 4.

2. THE ONE-DIMENSIONAL TRANSVERSE SPACE

In this section we study walks whose transverse space is one-dimensional. We first concentrate on the moments $\langle x^m(t)\rangle$, which, making use of Eq. (2), we can write as[17–21]

$$\langle x^m(t)\rangle = \left\langle \left\{ \int_0^t v[y(t')]\, dt' \right\}^m \right\rangle \tag{4}$$

Here the averages are first taken over the walks and then over the configurations, $\langle\cdot\rangle \equiv \langle\langle\cdot\rangle_w\rangle_c$. Introducing time-ordered variables, we have that Eq. (4) takes the form:

$$\langle x^m(t)\rangle = m! \int_0^t dt_1 \int_0^{t_1} dt_2 \cdots \int_0^{t_{m-1}} dt_m \,\langle\langle v[y(t_1)]\cdots v[y(t_m)]\rangle_w\rangle_c \tag{5}$$

The two type of averages in Eq. (5) factorize, so that

$$\begin{aligned}\langle\langle v[y(t_1)]\cdots v[y(t_m)]\rangle_w\rangle_c &= \int_{-\infty}^{\infty} dy_1 \cdots dy_m \,\langle v(y_1)\cdots v(y_m)\rangle_c \\ &\quad \times p(y_m, t_m)\, p(y_{m-1}-y_m, t_{m-1}-t_m)\cdots p(y_1-y_2, t_1-t_2)\end{aligned} \tag{6}$$

where $p(y, t)$ is the propagator in the y direction. Inserting (6) into (5), we observe that the integrations over the time variables are convolutions; thus in Laplace space Eq. (5) simplifies to

$$\langle x^m(u)\rangle = \frac{m!}{u}\int_{-\infty}^{\infty} dy_1\, dy_2 \cdots dy_m \,\langle v(y_1)\, v(y_2)\cdots v(y_m)\rangle_c \times p(y_m, u)\, p(y_{m-1}-y_m, u)\cdots p(y_1-y_2, u) \tag{7}$$

In ref. 21 we developed a detailed description for the calculation of the second and the fourth moments. In the Appendix of this paper we present a method with which the moments can be determined. Here we give the result for the mean-squared displacement:

$$\langle x^2(t)\rangle = (4/3)(2/\pi)^{1/2}\, t^{3/2} \tag{8}$$

where the exponent $\alpha = 3/2$ agrees with that obtained by Matheron and de Marsily.[14] The prefactor agrees with that given in ref. 21 when the transformation from dimensionless to regular units is performed.

An alternative way to derive the second moment is based on $N(y, t)$, the number of times the layer y has been visited up to time t. For a discrete y-lattice the displacement reads:

$$x(t) = \sum_y v(y)\, N(y, t) \tag{9}$$

A typical distribution for $N(y, t)$ is shown in Fig. 2, where $N(y, t)$ is plotted vs. y for a particular realization of the random walk after 10,000

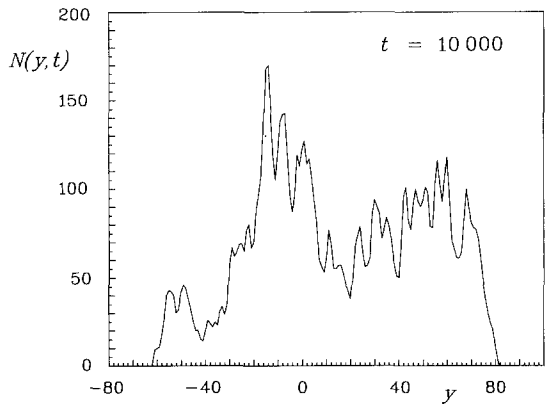

Fig. 2. A typical realization of the $N(y, t)$ distribution: Plotted is $N(y, t)$ vs. y after 10,000 time steps.

time steps. Obviously, the total number of visits is equal to the time t: $\sum_y N(y, t) = t$. From expression (9) we obtain for the mean squared displacement

$$\langle x^2(t) \rangle = \left\langle \left[\sum_y v(y)\, N(y, t) \right]^2 \right\rangle_{\mathrm{w,c}} \tag{10}$$

which, taking the average over the velocity configurations, yields

$$\langle x^2(t) \rangle = \left\langle \sum_y N^2(y, t) \right\rangle_{\mathrm{w}} \tag{11}$$

Now we introduce the distribution function $V^N(t)$, which denotes the average number of layers (sites) visited exactly N times in time t. Observing that the right-hand side of Eq. (11) is just the second moment of the $V^N(t)$ distribution, we may write

$$\langle x^2(t) \rangle = \sum_N N^2 V^N(t) \tag{12}$$

Up to this point the derivation of the alternative representation is general and applies for any transverse space. We continue focusing on the one-dimensional case and use the generating function technique which is based on fixed stepping times τ so that the number of steps is $n = t/\tau$. The generating function of an arbitrary function $f(n)$ is then defined by $f(z) = \sum_n z^n f(n)$, where z is the generating function variable. The generating function of $V^N(t)$ then is[25]

$$V^N(z) = \frac{1}{(1-z)^2\, p(0, z)} \left[1 - \frac{1}{p(0, z)} \right]^{N-1} \tag{13}$$

where $p(0, z)$ is the propagator of the one-dimensional motion. The second moment can now be calculated readily so that the generating function for the mean squared displacement is

$$\langle x^2(z) \rangle = (1-z)^{-2} \left[2p(0, z) - 1 \right] \tag{14}$$

Inserting the corresponding expression for the 1D propagator[25]

$$p(0, z) = (1 - z^2)^{-1/2} \tag{15}$$

into Eq. (14), one has

$$\langle x^2(z) \rangle = (1-z)^{-2} \left[2(1 - z^2)^{-1/2} - 1 \right] \tag{16}$$

which upon backtransformation to the time domain gives to first order

$$\langle x^2(t)\rangle = (4/3)(2/\pi)^{1/2}\, t^{3/2} + \cdots \tag{17}$$

Here we notice the agreement between Eqs. (8) and (17), which were derived along different paths.

In Fig. 3 we demonstrate how the exponent and the prefactor fit the results obtained from numerical realizations based on Eq. (11). Distinct from ref. 21, here the steps along a particular layer y are chosen to follow exactly the number of visits to that layer; in ref. 21 a two-dimensional system was considered where the steps were chosen randomly either along a pregiven x direction or along the positive or negative y direction. Averages are taken over 10^4 realizations. Plotted in the upper part of the figure is the observed exponent $\partial \ln\langle x^2(t)\rangle/\partial \ln t$ versus t. The convergence of the simulated exponent to the theoretical value of $\alpha = 3/2$ (indicated by a dashed line) is rather fast. The prefactor is analyzed in the lower part of the figure. Plotted is $\langle x^2(t)\rangle/t^{3/2}$ versus t. The computed prefactor converges to a constant value, which agrees well with the theoretical prediction of Eqs. (8) and (11): $(4/3)(2/\pi)^{1/2} \simeq 1.064$. The latter is indicated by the lower dashed line. Furthermore, the figure here is very similar to the one presented in ref. 21.

Generally, the moments follow the power law

$$\langle x^{2m}(t)\rangle = C_{2m}\, t^{3m/2} \tag{18}$$

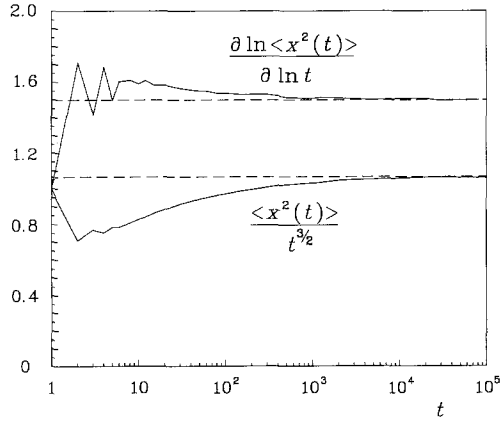

Fig. 3. The mean-squared displacement $\langle x^2(t)\rangle$ for longitudinal motion. In the upper part of the figure the effective exponent, given by $\partial \ln\langle x^2(t)\rangle/\partial \ln t$, is plotted versus t, as indicated. The upper dashed line represents the theoretical value $\alpha = 3/2$. In the lower part $\langle x^2(t)\rangle/t^{3/2}$ is plotted. The lower dashed line gives the theoretical value of $(4/3)(2/\sqrt{\pi})$, see text for details.

which is obtained from the Laplace inversion of Eq. (A4). The prefactors C_{2m} calculated on the basis of Eqs. (A4) and (A21) are listed in Table I. We define the reduced moments

$$M_{2m} = \langle x^{2m}(t) \rangle / \langle x^2(t) \rangle^m \tag{19}$$

which are given as numerical results in Table I.

We now turn to the evaluation of the propagator $P(x, t)$, the probability to be at x at time t, having started at the origin at $t = 0$. Since the system has different characteristics of motion in the longitudinal and in the transverse directions, the natural description which we follow is also based on different quantities for each direction. In the x direction the mean-squared displacement $\langle x^2(t) \rangle$ is the relevant quantity, while in the y direction the mean number of layers visited $\langle R(t) \rangle$ is the relevant quantity, as will become obvious in the following. Correspondingly, two scaling variables may be defined. Since $\langle x^2(t) \rangle \sim t^{3/2}$, we set

$$\xi = x/t^{3/4} \tag{20a}$$

and since $\langle R(t) \rangle \sim t^{1/2}$, we set

$$\rho = R/\sqrt{t} \tag{20b}$$

In order to write the propagator in terms of ξ and ρ, we focus on $N(y, t; R)$, which gives the conditional number of visits to layer y provided that the walker has visited R layers in time t. Accordingly, the conditional displacement for a walk having visited exactly R layers is

$$x(t; R) = \int_{-\infty}^{\infty} dy\, v(y)\, N(y, t; R) \tag{21}$$

Table I. Quantities Relevant for the Moments of the One-Dimensional Transverse Space[a]

$2m$	$\sum_{\{\mathbf{P}\}} A(\mathbf{P})$	C_{2m}	M_{2m}	$\tilde{M}_{2m}$
2	2/1	1.06	1.0	1.0
4	22/3	3.67	3.240	3.242
6	1345/36	22.71	18.86	18.82
8	32678/135	211.80	165.35	163.46
10	246852010/129600	2720.67	1996.56	1939.38
12	30062176657/1701000	45563.81	31430.21	29726.37

[a] $2m$ denotes the degree of the moment, $\sum_{\{\mathbf{P}\}} A(\mathbf{P})$ is calculated from Eq. (A21), C_{2m} is the prefactor in Eq. (18), the exact reduced moment M_{2m} is defined in Eq. (19), and the approximate moment $\tilde{M}_{2m}$ is obtained from Eq. (40).

The conditional mean squared displacement is then

$$\langle x^2(t; R)\rangle = \left\langle \int dy\, N^2(y, t; R) \right\rangle_{w(R)} \tag{22}$$

where the average is taken over the reduced set $w(R)$ of walks for which exactly R layers are visited in time t. In principle, the right-hand side of Eq. (22) can be given in terms of the average of a squared quantity, which we approximate by the square of the average $\bar{N}(t; R)$, so that

$$\langle x^2(t; R)\rangle = R\overline{N^2(r; R)} \simeq \tilde{C}R[\bar{N}(t; R)]^2 \tag{23}$$

where $\tilde{C}$ is a constant of order unity. From the fact that $\bar{N}(t; R)$ is just the mean number of visits to a layer, provided that totally R layers are visited, it follows that $\bar{N}(t; R) = t/R$. Thus,

$$\langle x^2(t; R)\rangle \simeq \tilde{C}t^2/R \tag{24}$$

Taking the average over the R distribution, we again obtain the mean squared displacement:

$$\langle x^2(t)\rangle = \langle x^2(t; R)\rangle_R \sim \tilde{C}t^2\langle R^{-1}\rangle_R \sim t^{3/2} \tag{25}$$

where the last step follows from the relation $\langle R^{-1}\rangle \sim t^{-1/2}$.

The exact distribution of $x(t)$ is not known; however, to obtain an approximate $P(x, t)$, we may well assume that the conditional displacement $x(t; R)$ is Gaussian-distributed: At long times there is a sufficiently large number of $N(y, t; R)$ of similar magnitude (see Fig. 2) so that the average over the velocity (sign) configurations can be seen as being a large sum of independent, equally-distributed quantities, for which the central limit theorem applies. Then the conditional propagator is Gaussian:

$$P(x, t; R) \simeq \frac{p_R(R, t)}{[2\pi\langle x^2(t; R)\rangle]^{1/2}} \exp\left[-\frac{x^2}{2\langle x^2(t; R)\rangle}\right] \tag{26}$$

Here $p_R(R, t)$ is the probability to visit exactly R layers in time t.[25] Introducing ξ and ρ, Eqs. (20), into Eq. (26) gives

$$P(\xi, \rho) \simeq (2\pi\tilde{C})^{-1/2}\, p_\rho(\rho)\, \sqrt{\rho}\, \exp(-\xi^2\rho/2\tilde{C}) \tag{27}$$

where $P(\xi, \rho)$ and $p_\rho(\rho)$ are the rescaled functions corresponding to $P(xt^{3/4}, t; Rt^{1/2})\, t^{5/4}$ and $p_R(R\sqrt{t}, t)\sqrt{t}$. The propagator $P(\xi)$ follows now by integration over ρ, which we denote by the average

$$P(\xi) \simeq \langle(\rho/2\pi\tilde{C})^{1/2} \exp(-\xi^2\rho/2\tilde{C})\rangle_\rho \tag{28}$$

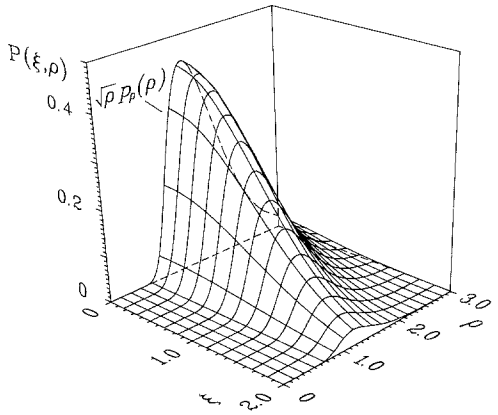

Fig. 4. Three-dimensional presentation of the $P(\xi, \rho)$ function. Plotted schematically is $P(\xi, \rho)$ versus the two variables ξ and ρ. See text for details.

To demonstrate the dependence of $P(\xi, \rho)$ on the two variables, we depict $P(\xi, \rho)$ schematically as a 2D surface in Fig. 4. The profiles along the ξ axis follow Gaussian distributions with variances depending on ρ: $\sigma^2 = \tilde{C}/\rho$. The profiles along the ρ direction are proportional to $p_\rho(\rho)\sqrt{\rho}$.

In Fig. 5 we show simulation calculation results. Plotted are the ratios $P(x, t; R)/P(0, t; R)$ versus $\xi\sqrt{\rho}$, accoding to the scaling relationship presented in Eq. (26). The numerical curves (which were slightly smoothed for small $\xi\sqrt{\rho}$ values) collapse to one single master curve. We found that

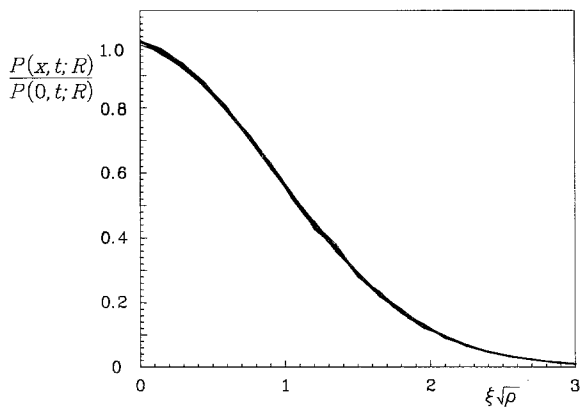

Fig. 5. Scaling relationship of the $P(x, t; R)$. Plotted is the ratio $P(x, t; R)/P(0, t; R)$ vs. $\xi\sqrt{\rho}$ for various R values and for the time kept fixed at $t = 1000$.

this master curve follows closely a Gaussian; results of this analysis are not depicted in the figure.

Turning now to the resemblance between the problem treated here and the trapping problem, we notice that in Eq. (28) the variable ρ appears linearly in the exponent. Thus, this form is very similar to those encountered in the trapping problem. The resemblance becomes more apparent when we substitute $\lambda = (\xi^2/2\tilde{C})$ in Eq. (28), so that

$$P(\xi) \sim \langle \sqrt{\rho}\, e^{-\lambda R} \rangle_\rho = \langle \exp(-\lambda\rho + \tfrac{1}{2} \ln \rho) \rangle_\rho \simeq \langle e^{-\lambda\rho} \rangle_\rho \tag{29}$$

where the last equality holds approximately for large λ. The last term on the right-hand side of Eq. (29) has been the subject of many studies and it has been found that the rare events dominate the asymptotic decay behavior[26–35] and that the Donsker–Varadhan[26] limit applies for the limiting large-λ behavior.

The resemblance of the motion in layered media and of the trapping problem appears also for the probability of a stretched-out walk. For these, $x(t)$ reaches the extreme value, $x = t$, for which the walk takes place on layers of equal orientation. The probability to have layers of equal orientation drops as $(1/2)^{R-1}$, where R, as given above, is the number of layers visited. Thus, the probability to stay on layers of equal signs follows the relation

$$P(x, t \simeq x) \sim \langle (1/2)^R \rangle_R \tag{30}$$

which corresponds to the trapping survival probability with trap concentrations of 1/2.[27] Again for large x the Donsker–Varadhan[26] limit applies, which leads to the decay

$$P(x, t \simeq x) \sim \exp(-Cx^{1/3}) \tag{31}$$

Following the methods developed for the trapping problem,[26–35] we determine here the asymptotic forms for the small- and large-ξ behavior of $P(\xi)$ at long times. For small ξ we obtain from a first-cumulant-type approximation[27]

$$P(\xi) \simeq (\langle \rho \rangle / 2\pi\tilde{C})^{1/2} \exp(-\xi^2 \langle \rho \rangle / 2\tilde{C}) \tag{32}$$

so that for small x

$$P(x, t) \sim a_0 t^{-3/4} \exp(-a_1 \xi^2) \tag{33}$$

where the constants are $a_0 = 2^{1/4}\pi^{-3/4}\tilde{C}^{-1/2}$ and $a_1 = (2/\pi)^{1/2}/\tilde{C}$. For large ξ we make use of the exact representation of the $p_\rho(\rho)$ distribution[25]:

$$p_\rho(\rho) = 8\rho^{-3} \sum_{j=1} [\pi^2 (2j+1)^2 \rho^{-2} - 1] \exp[-(2j+1)^2 \pi^2 / 2\rho^2] \tag{34}$$

Following refs. 34 and 36, we apply the method of steepest descent, which results in

$$P(\xi) \simeq b_0 t^{-3/4} \xi^{5/3} \exp(-\tilde{\xi}/2) \left(1 + \sum_{j=1}^{\infty} b_j / \tilde{\xi}^j\right) \tag{35}$$

with $\tilde{\xi} = 3 \cdot 2^{-1/3} (\pi/\tilde{C})^{2/3} \xi^{4/3}$ and where the first b_j constants are $b_0 = 2^{17/6} \pi^{-2/3} 3^{-1/2} \tilde{C}^{-4/3}$, $b_1 = 29/24$, $b_2 = 745/1152$, and $b_3 = -26155/82944$. Equations (33) and (35) may be cast in one single scaling form:

$$P(x, t) \sim t^{-3/4} f(\xi), \qquad \xi \sim x/t^{3/4} \tag{36}$$

with

$$f(\xi) \sim \begin{cases} \exp(-C_1 \xi^2) & \text{for small } \xi \quad (37a) \\ \xi^{5/3} \exp(-C_2 \xi^{4/3}) & \text{for large } \xi \quad (37b) \end{cases}$$

The scaling function $f(\xi)$ turns out to show a complicated crossover behavior. Only asymptotically, for very large ξ, does the function $f(\xi)$ follow a stretched Gaussian behavior with an exponent 4/3, as will be illustrated below in Fig. 8. Here we stress again that Eq. (35) holds in a limited x regime only; for $x > t$, $P(x, t)$ drops to zero. For a stretched-out walk we insert $t = x$ into Eq. (37b) and obtain the exponential term $\exp(-Cx^{1/3})$, which agrees with the form given in Eq. (31).

From the approximate representation of $P(x, t)$ we may derive approximate moments and compare them to the exact ones. We consider Eq. (27) and calculate the moments of the scaling variable ξ:

$$\begin{aligned} \langle \xi^{2m} \rangle &= \int d\xi \, \xi^{2m} P(\xi) \\ &= (2\pi\tilde{C})^{-1/2} \, 2 \int d\rho \, p_\rho(\rho) \sqrt{\rho} \int d\xi \, \xi^{2m} \exp(-\xi^2 \rho / 2\tilde{C}) \\ &= (2m-1)!! \, \tilde{C}^m \langle \rho^{-m} \rangle_{\mathrm{w}} \end{aligned} \tag{38}$$

where $(2m-1)!!$ denotes the double factorial $(2m-1)!! = 1 \cdot 3 \cdot 5 \cdots (2m-1)$. From the distribution given in Eq. (34) the negative moments $\langle \rho^{-m}(t) \rangle_{\mathrm{w}}$ can be calculated analytically:

$$\begin{aligned} \langle \rho^{-m} \rangle &= \int_0^\infty d\rho \, p_\rho(\rho) \, \rho^{-m} \\ &= 8 \cdot 2^{-m/2} (m+1)(1 - 2^{-m-2}) \, \pi^{-m-1} \Gamma(1 + m/2) \, \zeta(2+m) \end{aligned} \tag{39}$$

where ζ is the Riemann zeta function. Expectation values are given in Table I. The reduced approximate moments, which we denote by a tilde to distinguish them from the exact expressions, can be written in a simple closed form:

$$\tilde{M}_{2m} = \langle \xi^{2m} \rangle / \langle \xi^2 \rangle^m = (2m-1)!! \, \langle \rho^{-m}(t) \rangle \langle \rho^{-1}(t) \rangle^{-m} \tag{40}$$

The results of these moments are also collected in Table I. We observe that there is a very good agreement between the exact and approximate moments for low-order moments and that the agreement is better than 6% up to the 12th moment. This supports our assumption that $x(t; R)$ can be well described by a Gaussian and that, according to Eq. (24), $\langle x^2(t; R) \rangle \sim t^2/R$.

Note that the coefficients a_i and b_i in Eqs. (33) and (35) depend on $\tilde{C}$, which is the only unknown quantity. We may determine $\tilde{C}$ by equating the mean-squared displacement given in Eq. (17) and the second moment obtained from Eq. (40). This results in

$$\tilde{C} = \tfrac{4}{3}(2/\pi)^{1/2} \langle \rho^{-1} \rangle^{-1} = 1.564 \tag{41}$$

In Fig. 6 we present $\langle x^2(t; R) \rangle$ as obtained from simulation calculations for which averages are taken over 10^4 orientation configurations and over 10^4 random walk realizations. In order to test the functional

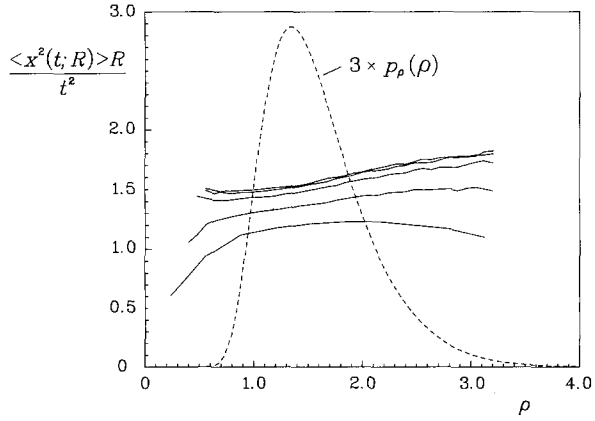

Fig. 6. The functional dependence of $\langle x^2(t; R) \rangle$. Full lines are the simulation results plotted as $\langle x^2(t; R) \rangle R/t^2$ vs. ρ. The number of time steps is given parametrically; the values are, from bottom to top: $t = 10$, 10^2, 10^3, 10^4, and 10^5. The dashed line represents the theoretical $p_\rho(\rho)$, Eq. (34).

dependence of $\langle x^2(t; R)\rangle$ on its arguments, we plotted $\langle x^2(t; R)\rangle R/t^2$ versus ρ with t as parameter. We choose this type of presentation, because if Eq. (24) holds exactly, the curves would follow horizontal lines. Furthermore, we have to connect the $\langle x^2(t; R)\rangle$ to the $p_\rho(\rho)$ distribution, Eq. (34), to depict the relevant range for $\langle x^2(t; R)\rangle$. The simulated curves deviate from horizontal lines and the deviations are larger for larger ρ values. However, in the small-ρ regime [relevant for the calculation of $P(x, t)$ at large x] we observe that the curves follow horizontal lines closely. We also observe that at long times the curves fall on top of each other within the numerical accuracy, which indicates a tendency to scaling at long times. Furthermore, the curves center around a value close to 1.5, which is in reasonable agreement with the theoretical result $\tilde{C} \simeq 1.56$, Eq. (41). All this is in good agreement with the analytical approach presented in this paper.

To give further justification to the assumption that the $x(t; R)$ are Gaussian-distributed, we plot in Fig. 7 the ratio $\langle x^4(t; R)\rangle/\langle x^2(t; R)\rangle^2$, which should take the value 3 for Gaussian distributions. We see that for larger times the curves converge toward an asymptotic form, again indicating scaling; moreover, some minor systematic deviations with a tendency to values larger than 3 are noticeable, mostly close to the center of the relevant regime, which is again indicated through the $p_\rho(\rho)$ distribution. However, for small ρ values, the important range for the calculation of the wings of $P(x, t)$, the ratio is quite close 3.

In Fig. 8 we compare the simulated and the theoretical distributions

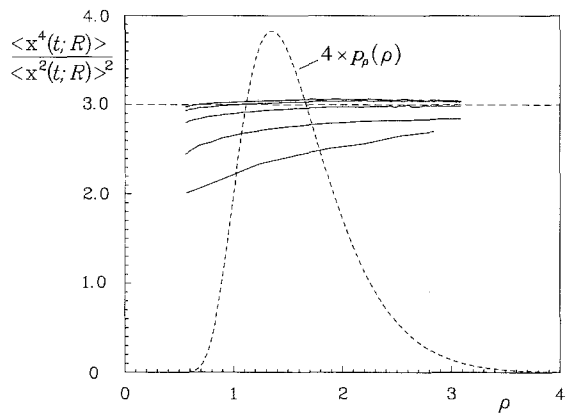

Fig. 7. Excess of the $x(t; R)$ distribution. Plotted is the ratio $\langle x^4(t; R)\rangle/\langle x^2(t; R)\rangle^2$ vs. ρ. The number of time steps is given parametrically; the values are, from bottom to top: $t = 10$, 10^2, 10^3, 10^4, and 10^5. The dashed line represents the theoretical $p_\rho(\rho)$, Eq. (34).

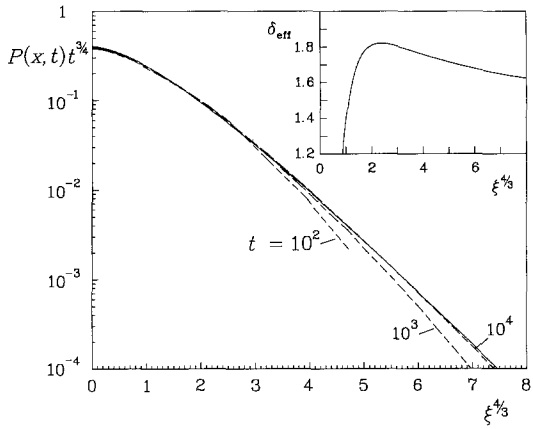

Fig. 8. The propagator $P(x, t)$. The dashed lines are the simulation results plotted as $P(x, t)\, t^{3/4}$ on a log scale versus $\xi^{4/3}$, where ξ is the scaling variable: $\xi = x/t^{3/4}$. The number of time steps t is given parametrically, as indicated. The full line is the theoretical result, obtained from Eqs. (33) and (35). The insert shows the effective exponent for the same ξ interval; see text for details.

$P(x, t)$. Again averages were taken over 10^4 orientation configurations and 10^4 random walk realizations. Plotted is $P(x, t)\, t^{3/4}$ on a logarithmic scale versus $\xi^{4/3}$ with t as parameter. The dashed lines are the results of the simulation calculations, and the full line depicts the theoretical finding of Eqs. (33) and (35), where a suitable ξ is chosen for the crossover. At longer times the simulation results follow the theoretical curve over a larger ξ range; this is due to the fact that at longer times the drop of $P(x, t)$ to zero occurs at progressively larger x values. In accordance to the findings of Fig. 6, the constant $\tilde{C}$ was chosen to be $\tilde{C} = 1.53$, slightly smaller than the value given in Eq. (41). For larger ξ the propagator $P(x, t)$ depends sensitively on the value of the constant $\tilde{C}$; the agreement between the simulation result for $t = 10^4$ and the theoretical curve is better when one uses $\tilde{C} = 1.53$ instead of $\tilde{C} = 1.56$. Again there are some minor differences from the corresponding figure of ref. 21, due to the slightly different models used.

The curves in Fig. 8 would follow straight lines if they obeyed a simple stretched Gaussian behavior $P(x, t) \sim \exp(-C\xi^{4/3})$; however, only asymptotically, for very small $P(x, t)$ one may expect to attain this behavior. To highlight this fact, we plot in the insert of Fig. 8 the effective exponent: $\partial \ln\{-\ln[P(x, t)/P(0, t)]\}/\partial \ln t$, where $P(x, t)$ is calculated from Eqs. (35). We observe that at ξ values for which $P(x, t)$ has decayed by almost four orders of magnitude, the exponent is still 1.63, clearly above the asymptotic value of 4/3. This finding documents the similarity between

the trapping and the diffusion problem.[34] Both show very slow convergence to a simple stretched exponential and for both problems one lacks a simple expression which would hold in the whole range of ξ values.

3. GENERALIZATION

Here we generalize the results of Section 2 to motion in higher-dimensional transverse spaces, such as, e.g., a square lattice (see Fig. 1b) or fractals. For fractals we use as example a Sierpinski gasket, so that the x axis is perpendicular to the gasket. The resulting structure was called Toblerone[35] and is illustrated in Fig. 1c. Another example for a transverse space is a system with hierarchically arranged barriers (or more generally, with hierarchically arranged connections between layers). This is illustrated in Fig. 1d, where the transverse connections represent an ultrametric space (UMS).

We first concentrate on the mean-squared displacement. Due to the spatial δ correlation of the velocities, Eq. (3), the temporal velocity correlation function measures the probability to be at the origin. Hence[16]

$$C_v(t) = \langle v(t)\, v(t=0) \rangle_w \sim p(0, t) \tag{42}$$

where $p(0, t)$ is the propagator of the diffusional motion in the transverse space. Generally, $p(0, t)$ is known to follow the power law

$$p(0, t) \sim t^{-d/2} \tag{43}$$

but we consider also fractals and UMS, for which[35]

$$p(0, t) \sim \begin{cases} t^{-\tilde{d}/2} & \text{for fractals} \\ t^{-\gamma} & \text{for UMS} \end{cases} \tag{44}$$

Here $\tilde{d}$ denotes the spectral dimension for fractals and is equal to the Euclidean dimension for regular lattices. γ is the exponent resulting from thermally activated transitions on UMS: $\gamma = (kT/\Delta) \ln z$, with T being the temperature, Δ the energy-level spacing, and z the branching ratio of the tree. The mean-squared displacement follows from the double integration:

$$\langle x^2(t) \rangle = \int_0^t dt' \int_0^t dt'' \, \langle v(t')\, v(t'') \rangle = 2 \int_0^t dt' \, (t - t')\, C_v(t') \tag{45}$$

Inserting Eqs. (42) and (44) into Eq. (45), we obtain

$$\langle x^2(t) \rangle = \begin{cases} t^{2-\tilde{d}/2}, & \tilde{d} < 2 \\ t \ln t, & \tilde{d} = 2 \\ t, & \tilde{d} > 2 \end{cases} \tag{46}$$

More generally and following the one-dimensional case, we consider the two relevant scaling variables; from $\langle x^2(t)\rangle \sim t^{\alpha}$ we set

$$\xi = x/t^{\alpha/2} \tag{47a}$$

and from $\langle R(t)\rangle \sim t^{\beta}$ we set

$$\rho = R/t^{\beta} \tag{47b}$$

In Eqs. (47) the exponent for the mean number of sites visited is

$$\beta = \begin{cases} \min(\tilde{d}/2, 1) & \text{for fractals} \\ \min(\gamma, 1) & \text{for UMS} \end{cases} \tag{48}$$

for which we may write

$$\alpha = 2 - \beta \tag{49}$$

possibly up to logarithmic corrections for the marginal cases. We note that the exponent is bounded for fractals: $1 < \alpha < 3/2$, which means that expression (47a) interpolates between the pure Brownian motion with $\alpha = 1$ and the enhanced diffusion with $\alpha = 3/2$. For UMS the diffusion exponent covers the full range between Brownian motion and ballistic motion: $1 < \alpha < 2$. Brownian behavior occurs at high temperatures, for which each step practically leads to a new layer, while ballistic behavior results at very low temperatures, where the motion involves only a few layers.

Again following the derivation for the 1D case, we have for the propagator in terms of the two scaling variables

$$P(\xi) \sim t^{-\alpha/2} \langle \exp(-c\xi^2 \rho) \rangle_{\rho} \tag{50}$$

For small ξ we introduce the first cumulant:

$$\begin{aligned} P(\xi) &\sim t^{-\alpha/2} \exp(-c_1 \xi^2 \langle \rho \rangle) \\ &= t^{-\alpha/2} \exp(-c_2 x^2/t^{\alpha}) \end{aligned} \tag{51}$$

For large ξ we consider the Donsker–Varadham limit[26] and obtain for $\tilde{d} \leqslant 2$

$$\begin{aligned} P(x, t) &\sim t^{-\alpha/2} \exp[-c_3 \xi^{4/(\tilde{d}+2)}] \\ &= t^{-\alpha/2} \exp[-c_3 (x^4/t^{4-\tilde{d}})^{1/(\tilde{d}+2)}], \qquad \tilde{d} < 2 \end{aligned} \tag{52}$$

For $\tilde{d} \geqslant 2$ the analogy between trapping and the problem treated here fails: For trapping the long-time behavior is obtained from the survival

probability within an absorbing sphere irrespective of whether all sites within the sphere have been visited until absorption.[29] Here the number of layers visited is crucial and cannot be approximated by a spherical volume in the transverse space with a radius corresponding to the diffusion length. Thus the analogy works only for compact random walks, i.e., for the $\tilde{d}<2$ regime. In fact, for the probability of a stretched-out walk with strictly all steps in the same direction we obtain in analogy to the 1D case

$$P(x, t \simeq x) \sim \exp[-Cx^{\tilde{d}/(\tilde{d}+2)}] \tag{53}$$

Setting $t=x$, this expression reproduces that of Eq. (52). We thus conclude that for $\tilde{d}<2$, Eqs. (50) and (52) provide an appropriate description of $P(x, t)$. By analogy, we assume that scaling holds also for $\tilde{d}>2$, so that we have for large x

$$P(x, t) \sim \exp[-C(x^2/t)^{\tilde{d}/(\tilde{d}+2)}], \qquad \tilde{d}>2 \tag{54}$$

This expression equals that of regular diffusion only in the limit $\tilde{d} \to \infty$. In other words, we recover ordinary diffusion behavior in the limit when each step leads to a new layer and the correlation between the x orientations of successive steps is zero. Collecting the results of Eqs. (50), (52), and (54), we obtain the scaling form

$$P(x, t) \sim t^{-\alpha/2} e^{-c\xi^{\delta}}, \qquad \xi \sim x/t^{\alpha/2} \tag{55}$$

where

$$\delta = \begin{cases} 2 & \text{for small } \xi \quad (56a) \\ 2 \max(2, \tilde{d})/(\tilde{d}+2) & \text{for large } \xi \quad (56b) \end{cases}$$

where the last expression is a conjecture for the case of $\tilde{d}>2$; furthermore, $P(x, t)$ is zero for $x>t$, so that Eqs. (55) and (56) are approximate.

5. CONCLUSIONS

In this paper we studied the enhanced diffusion due to convection in random velocity fields, also connecting the problem to trapping. For one-dimensional transverse motion we reported the exact calculation of the moments of the displacements. The propagator $P(x, t)$ depends on two relevant quantities, due to differences in the motion in the longitudinal and transverse directions, respectively. Enhanced diffusion bears a close relationship to trapping: thus we could apply the methods developed for trapping to derive long-time asymptotic forms for $P(x, t)$ both for small and large x values. $P(x, t)$ shows a stretched Gaussian pattern characterized by a complex crossover behavior and slow convergence to the asymptotic forms. We supported our analytical findings by simulation calculations.

We also generalized the model to higher-dimensional transverse motion, and again used two scaling variables. Here the analogy to trapping holds closely as long as the dimensionality of the transverse space is less than two. For space dimensions larger than two the scaling form presented by us for large x values is a conjecture.

There is a further analogy between the results presented in this work and those obtained for Lévy walks.[8–13] Lévy walks were used to describe both dispersive and enhanced diffusion. The situation is similar here, in that we obtain enhanced diffusion readily. Interestingly, there is a basic difference between the models: Lévy walks are related to continuous-time random walks (CTRW), based on waiting-time probabilities which (distinct from the layered models presented here) are independent of the particle location. In the classical CTRW framework the waiting-time probabilities show power-law decays in space and time, from which (for small exponents) enhanced diffusion follows. On the other hand, in the model treated in this paper the displacements depend heavily on the organization of the velocities in the layers and the averages also involve the particular velocity configurations. The enhanced diffusion stems mainly from the strong sample-to-sample fluctuations.

On a more technical note, we stress that care is required when determining asymptotic forms; it is often useful to go beyond the exponential part of the saddlepoint approximation, because accounting for power-law exponential prefactors is often necessary for obtaining a satisfactory agreement between analytical and numerical results. This is in line with previous findings for related problems[34,37] and we used this knowledge here to highlight the crossover to the asymptotic stretched Gaussian behavior.

Summarizing, both diffusion in random velocity fields and Lévy walks offer many appealing aspects in describing enhanced diffusion; both models start from an underlying microscopic physical picture, but also for both models the connection to a first-principles understanding of enhanced diffusion is still rudimentary.

APPENDIX

In this Appendix we derive a closed-form expression which allows the exact calculation of the moments for the displacements in the Laplace space. We begin by rewriting Eq. (7) of the main text:

$$\langle x^m(t)\rangle = \frac{m!}{u}\int_{-\infty}^{\infty} dy_1\, dy_2 \cdots dy_m\, \langle v(y_1)\, v(y_2) \cdots v(y_m)\rangle_c \times p(y_1, u)\, p(y_2 - y_1, u) \cdots p(y_m - y_{m-1}, u) \tag{A1}$$

and consider for $p(y, u)$ the one-dimensional solution of the propagator:

$$p(y, u) = (2u)^{-1/2} \exp[-|y|\,(2u)^{1/2}] \tag{A2}$$

As mentioned in the main text, dimensionless units are used, i.e., lengths are given in units of a, time in units of τ, and the velocities in units of a/τ. Since the velocities are δ-correlated [Eq. (3) of the main text], one may write the configurational-dependent term of the integrand in Eq. (A1) as

$$\langle v(y_1) \cdots v(y_m) \rangle_c = \sum_{\{\mathbf{P}\}} \delta(y_{P_1} - y_{P_2})\, \delta(y_{P_2} - y_{P_3}) \cdots \delta(y_{P_{m-1}} - y_{P_m}) \tag{A3}$$

where $\mathbf{P}$ denotes a particular permutation of the indices $\{1, 2, \ldots, m\}$ and the sum runs over all possible permutations $\{\mathbf{P}\}$. Inserting (A2) and (A3) into (A1) and substituting $\tilde{y}_j$ for $y_j(2u)^{1/2}$, one has

$$\begin{aligned}\langle x^m(u) \rangle &= \frac{m!}{u(2u)^{3m/4}} \sum_{\{\mathbf{P}\}} \int_{-\infty}^{\infty} d\tilde{y}_1\, d\tilde{y}_2 \cdots d\tilde{y}_m \\ &\quad \times \delta(\tilde{y}_{P_1} - \tilde{y}_{P_2})\, \delta(\tilde{y}_{P_2} - \tilde{y}_{P_3}) \cdots \delta(\tilde{y}_{P_{m-1}} - \tilde{y}_{P_m}) \\ &\quad \times \exp(-|\tilde{y}_1| - |\tilde{y}_2 - \tilde{y}_1| - \cdots - |\tilde{y}_m - \tilde{y}_{m-1}|) \\ &= \frac{m!}{u(2u)^{3m/4}} \sum_{\{\mathbf{P}\}} A_m(\mathbf{P})\end{aligned} \tag{A4}$$

Because of the products of δ-functions, the $A_m(\mathbf{P})$ differ from zero only if there are pairs of like variables. From this it follows that $(m-1)!!$ possible realizations of pairs occur and that accordingly an equal number of $A_m(\mathbf{P})$ have to be calculated. Furthermore, the integration has to be taken only over half of the number of variables, which we denote by $z_1, z_2, \ldots, z_n$, $n = m/2$.

We now concentrate on the integrand and consider a zeroth set $\mathbf{P}$ of pairs of indices:

$$\{1, 1, 2, 2, \ldots, n, n\} \tag{A5}$$

for which the integrand reads

$$\exp(-|z_1| - |z_2 - z_1| - \cdots - |z_n - z_{n-1}|) \tag{A6}$$

Reordering the indices by interchanging the second and the third indexes, one has

$$\{1, 2, 1, 2, \ldots, n, n\} \tag{A7}$$

from which the integrand reads

$$\exp(-|z_1| - 3\,|z_2 - z_1| - |z_3 - z_2| - \cdots - |z_n - z_{n-1}|) \tag{A8}$$

Thus the $A_m(\mathbf{P})$ are of the general form

$$A_m(\mathbf{P}) = \int_{-\infty}^{\infty} dz_1 \cdots dz_n \exp\left(- |z_1| - \sum_{i<j}^{n} a_{ij}(\mathbf{P})\, |z_j - z_i| \right) \tag{A9}$$

where a_{ij} are integers and depend on $\mathbf{P}$. Although this integrand looks rather simple, it turns out that the integration is not trivial because of the absolute value terms which appear in the exponent. To solve the integral, we first eliminate the absolute value terms by splitting the integration ranges in the n-dimensional variable space, such that ordered sets of variables appear. Thus the integration has to be performed for ranges: $z_1 < z_2 < \cdots < z_n$; $z_2 < z_1 < z_3 < \cdots < z_n$; plus all other permutations of ordered sets of variables $z_1 \cdots z_n$.

Because z_1 appears also by itself in the exponent, we center the integration around z_1 and write

$$\begin{aligned} A_m(\mathbf{P}) = & \int_{-\infty}^{\infty} dz_1 \int_{z_1}^{\infty} dz_2 \cdots \int_{z_{n-1}}^{\infty} dz_n \exp\left[-|z_1| - \sum_{i<j}^{n} a_{ij}(\mathbf{P})(z_j - z_i) \right] \\ & + \int_{-\infty}^{\infty} dz_1 \int_{-\infty}^{z_1} dz_2 \int_{z_1}^{\infty} dz_3 \cdots \int_{z_{n-1}}^{\infty} dz_n \\ & \times \exp\left[-|z_1| + a_{12}(z_2 - z_1) - \sum_{\substack{i<j \\ i>2}}^{n} a_{ij}(\mathbf{P})(z_j - z_i) \right] \\ & + \{\text{integrals for all other possible permutations} \\ & \quad \text{of sets of ordered variables}\} \end{aligned} \tag{A10}$$

We now denote by $\mathbf{I}$ a particular permutation of the indices $\{1, 2, \ldots, n\}$ such that

$$z_{I_1} < z_{I_2} < \cdots < z_{I_{k-1}} < z_1 < z_{I_{k+1}} < \cdots < z_{I_n} \tag{A11}$$

with $I_k = 1$. We further denote by $\mathbf{J}$ the inverted permutation vector $\mathbf{I}$ so that

$$I_{J_j} = j \tag{A12}$$

Making use of the permutation vectors $\mathbf{I}$ and $\mathbf{J}$, one may write the integrals in Eq. (A10) as

$$\begin{aligned} A_m = & \sum_{\{\mathbf{I}\}} \int_{-\infty}^{\infty} dz_1 \int_{-\infty}^{z_1} dz_{I_{k-1}} \int_{-\infty}^{z_{I_{k-1}}} dz_{I_{k-2}} \cdots \\ & \times \int_{-\infty}^{z_{I_2}} dz_{I_1} \int_{z_1}^{\infty} dz_{I_{k+1}} \int_{z_{I_{k+1}}}^{\infty} dz_{I_{k+2}} \cdots \int_{z_{I_{n-1}}}^{\infty} dz_{I_n} \\ & \times \exp\left[-|z_1| - \sum_{i<j}^{n} a_{ij} \sigma_{J_i J_j} (z_j - z_i) \right] \end{aligned} \tag{A13}$$

where the sum runs over all possible permutations $\{\mathbf{I}\}$ and for simplicity we have omitted the permutation vector $\mathbf{P}$. The σ_{ij} takes values ± 1 according to the conditions

$$\sigma_{ij} = \begin{cases} 1, & j > i \\ -1, & j < i \end{cases} \tag{A14}$$

Substituting $\tilde{z}_j = z_{I_j}$ or equivalently $z_j = \tilde{z}_{J_j}$ into Eq. (A13), we have that the integrand simplifies to

$$\begin{aligned} A_m = \sum_{\{\mathbf{I}\}} & \int_{-\infty}^{\infty} d\tilde{z}_k \int_{-\infty}^{\tilde{z}_k} d\tilde{z}_{k-1} \int_{-\infty}^{\tilde{z}_{k-1}} d\tilde{z}_{k-2} \cdots \\ & \times \int_{-\infty}^{\tilde{z}_2} d\tilde{z}_1 \int_{\tilde{z}_k}^{\infty} d\tilde{z}_{k+1} \int_{\tilde{z}_{k+1}}^{\infty} d\tilde{z}_{k+2} \cdots \int_{\tilde{z}_{n-1}}^{\infty} d\tilde{z}_n \\ & \times \exp\left[-|\tilde{z}_k| - \sum_{i<j}^{n} a_{ij} \sigma_{J_i J_j} (\tilde{z}_{J_j} - \tilde{z}_{J_i}) \right] \end{aligned} \tag{A15}$$

The sum in the exponent can be rearranged so that

$$\exp\left[-|\tilde{z}_k| - \sum_{i<j}^{n} a_{I_i I_j} (\tilde{z}_j - \tilde{z}_i) \right] \tag{A16}$$

Collecting the coefficients for each integration variable, one has for the integrand

$$\exp\left(-|\tilde{z}_k| - \sum_{j=1}^{n} b_j \tilde{z}_j \right) \tag{A17}$$

with

$$b_i = -\sum_{j=1}^{n} a_{I_i I_j} \sigma_{ij} \tag{A18}$$

where the b_j depend on $\mathbf{P}$ through $a_{ij}(\mathbf{P})$. Observing that

$$\sum_{j=1}^{n} b_j = 0 \tag{A19}$$

the integration can be performed leading to

$$\begin{aligned} A_m = 2 \sum_{\{\mathbf{I}\}} & \frac{-1}{b_1} \frac{-1}{b_1 + b_2} \cdots \frac{-1}{b_1 + b_2 + \cdots + b_{k-1}} \\ & \times \frac{1}{b_n} \frac{1}{b_n + b_{n-1}} \cdots \frac{1}{b_n + b_{n-1} + \cdots + b_{k+1}} \end{aligned} \tag{A20}$$

This expression may be recast into

$$A_m = 2 \sum_{\{\mathbf{I}\}} \left[(-1)^{k-1} \left(\prod_{i=1}^{k-1} \sum_{j=1}^{i} b_j \right) \left(\prod_{i=k+1}^{n} \sum_{j=1}^{n} b_j \right) \right]^{-1} \tag{A21}$$

which is our final result. It thus follows that the calculation of the mth moment requires the sum of $(m-1)!!\,(m/2)!$ terms. The realization of the algorithm can be rendered machine-independent, being limited only by the computer time and by the number of digits of integer numbers available. The numerical results are presented in Table I.

ACKNOWLEDGMENTS

We thank F. Weber for technical assistance. A grant of computer time from the Rechenzentrum der ETH-Zürich and the support of the Deutsche Forschungsgemeinschaft (SFB 213) and of the Fonds der Chemischen Industrie are gratefully acknowledged. J.K. acknowledges the support of the Fund for Basic Research administrated by the Israel Academy of Sciences and Humanities.

REFERENCES

1. L. F. Richardson, *Proc. R. Soc. Lond. A* **110**:709 (1926).
2. G. K. Batchelor, *Proc. Camb. Phil. Soc.* **48**:345 (1952).
3. G. K. Batchelor and A. A. Townsend, in *Surveys in Mechanics*, G. K. Batchelor and R. M. Davies, eds. (Cambridge University Press, 1956), p. 352.
4. A. S. Monin and A. M. Yaglom, *Statistical Fluid Mechanics*, Vol. II (MIT, Cambridge, Massachusetts, 1971), Vol. II (1975).
5. A. Okubo, *J. Oceanol. Soc. Jpn.* **20**:286 (1962).
6. H. G. E. Hentschel and I. Procaccia, *Phys. Rev. A* **29**:1461 (1984).
7. T. Geisel, J. Nierwetberg, and A. Zacherl, *Phys. Rev. Lett.* **54**:616 (1985).
8. M. F. Shlesinger and J. Klafter, *Phys. Rev. Lett.* **54**:2551 (1985).
9. J. Klafter, A. Blumen, and M. F. Shlesinger, *Phys. Rev. A* **35**:3081 (1987).
10. G. Zumofen, A. Blumen, J. Klafter, and M. F. Shlesinger, *J. Stat. Phys.* **54**:1519 (1989).
11. A. Blumen, G. Zumofen, and J. Klafter, *Phys. Rev. A* **40**:3964 (1989).
12. A. Blumen, J. Klafer, and G. Zumofen, in *Dynamical Processes in Condensed Molecular Systems*, J. Klafter, J. Jortner, and A. Blumen, eds. (World Scientific, Singapore, 1989).
13. G. Zumofen, A. Blumen, and J. Klafter, *Chem. Phys.* **146**:433 (1990).
14. G. Matheron and G. de Marsily, *Water Resources Res.* **16**:901 (1980).
15. J.-P. Bouchaud, A. Georges, and P. Le Doussal, *J. Phys.* (Paris) **48**:1855 (1987).
16. R. M. Mazo and C. Van den Broeck, *J. Chem. Phys.* **86**:454 (1987).
17. S. Redner, *Physica D* **38**:287 (1989).
18. S. Redner, *Physica A* **168**:551 (1990).
19. J.-P. Bouchaud, A. Georges, J. Koplik, A. Provata, and S. Redner, *Phys. Rev. Lett.* **64**:2503 (1990).
20. J.-P. Bouchaud and A. Georges, *Phys. Rep.* **195**:127 (1990).
21. G. Zumofen, J. Klafter, and A. Blumen, *Phys. Rev. A* **42**:4601 (1990).

22. P. Le Doussal and J. Machta, *Phys. Rev. B* **40**:9427 (1989).
23. D. A. Darling and M. Kac, *Trans. Am. Math. Soc.* **84**:454 (1957).
24. M. Kac, *Trans. Am. Math. Soc.* **84**:459 (1957).
25. G. H. Weiss and R. J. Rubin, *Adv. Chem. Phys.* **52**:363 (1983).
26. M. D. Donsker and S. R. S. Varadhan, *Commun. Pure Appl. Math.* **28**:525 (1975); **32**:721 (1979).
27. G. Zumofen and A. Blumen, *Chem. Phys. Lett.* **88**:63 (1982).
28. B. Movaghar, G. W. Sauer, D. Würtz, and D. L. Huber, *Solid State Commun.* **39**:1179 (1981).
29. P. Grassberger and I. Procaccia, *J. Chem. Phys.* **77**:6281 (1982); *Phys. Rev. A* **26**:3686 (1982).
30. R. F. Kayser and J. B. Hubbard, *Phys. Rev. Lett.* **51**:79 (1983); *J. Chem. Phys.* **80**:1127 (1984).
31. J. Klafter, G. Zumofen, and A. Blumen, *J. Phys. Lett.* (Paris) **45**:L49 (1984).
32. G. Zumofen, A. Blumen, and J. Klafter, *J. Phys. A* **17**:L479 (1984).
33. G. H. Weiss and S. H. Havlin, *J. Stat. Phys.* **37**:17 (1984).
34. J. K. Anlauf, *Phys. Rev. Lett.* **52**:1845 (1984).
35. A. Blumen, J. Klafter, and G. Zumofen, in *Optical Spectroscopy of Glasses*, I. Zschokke, ed. (Reidel, Dordrecht, 1986), p. 199.
36. N. Agmon and M. L. Glaser, *Phys. Rev. A* **34**:656 (1986).
37. J. Klafter, G. Zumofen, and A. Blumen, *J. Phys. A*, in press.